Monitoring Polypropylene Chain-Scission for Dissolution-Based Recycling by In Situ Near Infrared and Raman Spectroscopy

Sofiane Ferchichi, Nida Sheibat-othman, Olivier Boyron, Sébastien Norsic, Maud Rey-bayle, Vincent Monteil

Macromolecular Rapid Communications, 2025, 2400748, 10.1002/marc.202400748

Monitoring Polypropylene Chain-Scission for Dissolution-based Recycling by *in-situ* Near Infrared and Raman spectroscopy

Sofiane Ferchichi[a,b,c], *Nida Sheibat-Othman*[b*], *Olivier Boyron*[c], *Sébastien Norsic*[c], *Maud Rey-Bayle*[a], *Vincent Monteil*[c*]

[a]IFP Energies Nouvelles, Rond-Point de l'échangeur de Solaize, 69360 Solaize, France
[b]Universite Claude Bernard Lyon 1, LAGEPP, UMR 5007, CNRS, 69622 Villeurbanne, France
[c]Universite Claude Bernard Lyon 1, CP2M, UMR 5128, CNRS, 69616 Villeurbanne, France
E-mail: Vincent.MONTEIL@univ-lyon1.fr, nida.othman@univ-lyon1.fr

Keywords: Polypropylene, Chain-scission, Recycling, Spectroscopy, Monitoring, GA-PLS

Abstract

Within the context of polypropylene recycling by dissolution, the potential degradation of polypropylene in solution has been investigated using in-situ NIR and Raman spectroscopy. Pure polypropylene, completely free of additives and commercial polypropylene, low in additives, are degraded on purpose under different conditions. Genetic algorithm combined with partial least squares (GA-PLS) models have been built based on NIR spectra, and partial least squares (PLS) models based on Raman spectra, to predict the mass average molar mass and the chain-scission rate, respectively, during the degradation process. The variables used in the GA-PLS model from NIR spectra suggest that the main variability is related to physical changes via the baseline. In Raman, a baseline drift due to coloration during the degradation has been used to correlate the spectra with the degradation phenomenon. Both techniques show good predictive performances and can potentially be implemented for real-time supervision of degradation during recycling processes.

1. Introduction

Solvent-based recycling emerge as a promising technique to manage plastic wastes. In this innovative purification approach, polymers are first dissolved in a suitable solvent, so allowing the extraction of additives and the recovery of valuable polymers from waste streams. The purified polymers can then be reprocessed into new materials, thus reducing the demand

of new polymers, and minimizing the environmental impact. The recovered virgin resin is capable of being reused in a wide range of applications. Indeed, the thermal, structural, and mechanical properties of the polymeric material do not change during the recycling process. This strategic use of polymer dissolution in recycling aligns with the principles of circular economy, promoting the closed-loop life cycle of polymers to enhance their overall sustainability.

While many polymers can be dissolved in various solvents at low temperatures, polyolefins do not fall into this category and their semi-crystalline character contributes to increasing their dissolution temperature. The mean temperatures used for the dissolution of LDPE, LLDPE/HDPE and PP are around 90°C, 100°C and 120°C respectively (depending on the solvent and polymer properties) [1–3], so the risk of degradation is high. The degradation phenomenon can result in the partial or complete breakdown of the polymer chain, particularly when exposed to specific environmental factors such as heat, oxygen and/or moisture, light, chemical environments, and bacterial action. [4]

Polyolefins degradation occurs mainly through two reactions: oxidation and chain scission. Polypropylene is known to be more fragile than polyethylene [5] and its thermal oxidation occurs because of the simultaneous effects of the high temperature and the presence of oxygen (mechanism detailed in Figure S1). [6] The oxidation mechanism starts at the weakest C-H bond of the propylene repeating unit of the polymer chain, [7] so forming radicals by H-abstraction (A). Then, in the presence of oxygen, a peroxy-radical is formed (B), followed by the formation of a hydroperoxide (C). Decomposition of this hydroperoxide leads either to the formation of oxidation products (in-chain ketones (D), end-chain ketones (E) or alcohol (F)) or to chain scission (G). In the absence of oxygen, the polypropylene macroradical obtained from H-abstraction will further evolve and also lead to cleavage by β scission ((A) to (G) directly). Note that cross-linking through the recombination of two radicals is also possible, but it is less reported in the literature and less probable due to the steric hindrance of the methyl group. [8] It has however been observed during gamma irradiation of PP samples, [9] which suggests that only very harsh conditions can lead to cross linking. Globally, polyethylene (PE) will follow the same degradation scheme as polypropylene, although the lower concentration of methine groups confers it a higher stability with regards to this degradation mechanism. [10] The degradation of PE can mainly start due to the presence of structural defect such as branching [11] or C=C bonds (vinyl in HDPE and vinylidene in LDPE). [12]

Different degradation conditions of polypropylene have been investigated in the literature. Degradation of polypropylene by radical-initiation has been conducted in a rheo-reactor [13] leading to a large decrease of chains lengths. The same tendency has been observed in water, in the case of microplastics in the sea. [14] In organic solvents, different authors studied the degradation mechanism by performing "controlled" degradation using peroxides [15]. They showed that at 150 °C in ortho-dichlorobenzene, in which PP is soluble, and depending on the peroxide type, the mass average molar mass can significatively decrease from 600 kg mol^{-1} to 300 kg mol^{-1}. The combination of the oxidative and chain scission phenomena of polypropylene has been investigated using a radical initiator and a metal catalyst, where even at relatively low temperature (75 °C) both phenomena were observed in chlorobenzene. [16]

The main method to characterize polypropylene degradation is the molar mass measurement by high temperature size exclusion chromatography (HT-SEC) before and after the experiment. Also, the carbonyl index is a good indicator to evaluate the oxidation level of polyolefins,[17–20] so it can be used to monitor their photo– or thermal degradation, for instance based on the absorption band of the carbonyl species by Attenuated total reflectance infrared (ATR-IR) spectroscopy. However, it was mainly calculated to evaluate the ageing of plastic waste in the environment or during processing or mechanical recycling, but not for the monitoring of the evolution of the polymer molar mass during its dissolution. Spectroscopic methods can also be helpful to monitor polymer degradation. For instance, authors[21] employed Raman spectroscopy to monitor the degradation of polypropylene based on changes in the molar mass at the exit of an extruder, after multiple extrusion cycles. They related the decrease in the intensities of the Raman bands of the C-C backbone to a reduction in chain length, and consequently, a decrease in molar mass.

In this work, we aim to monitor the degradation of polypropylene in solution using two spectroscopic techniques, near-infrared (NIR) and Raman spectroscopy. These techniques are particularly well-suited for this application due to their sensitivity to both chemical and physical changes and can be operated in-situ using probes. We attempt to extract molar mass information from the NIR and Raman spectra through multivariate regression. *Ex-situ* SEC molar mass data is used for calibrating the *in-situ* spectroscopic methods. In the broader context of our research on dissolution-based recycling, we explored various solvents to optimize the process like linear n-alkanes, cyclic alkanes, ketones or esters.[22] This study specifically focuses on 1,2,4-trichlorobenzene (TCB), chosen due to its favorable properties (optical and thermodynamic) reported in the literature. First, TCB is known for its good solubilization for non-polar polymers such as PP, allowing for effective dissolution at

elevated temperatures. Its high boiling point (214°C) ensures thermal stability, enabling degradation studies to be conducted without solvent evaporation or breakdown. Additionally, TCB is relatively chemically inert, minimizing the risk of side reactions during the degradation process, and allowing for a clear observation of the polymer's behavior. Moreover, TCB which does not contain any $-CH_2$ or $-CH_3$ groups, is optically clear in key spectral regions used in in-situ monitoring techniques such as Raman and NIR spectroscopy, enabling the direct observation of changes in polymer structure and molar mass without solvent interference. Finally, the close match between TCB's solubility parameters and those of PP facilitates homogenous dissolution and reduces phase separation, ensuring precise degradation analysis.

This methodology represents a significant advancement in the field of recycling by dissolution, as it enables real-time, *in-situ* monitoring of polypropylene chain scission and degradation. Compared to traditional methods, which rely on *ex-situ* analysis such as HT-SEC or carbonyl index measurements, this approach allows for more immediate and accurate monitoring of polymer degradation during the recycling process, leading to better process control and polymer recovery.

2. Experimental section

2.1. Polymer

Three different types of polymers have been considered in this study: aged virgin polymers, fresh virgin polymers and commercial polymers (slightly additive). The aim is to study the predictive performances of the spectroscopic techniques of the polymer properties, specifically in the context of recycling were the polymers coming from the waste stream contain additives and have potentially undergone some initial degradation.

- Aged virgin polypropylene (PP1), free of additives, has been synthesized in our laboratory using Ziegler-Natta catalysis. Different initial molar masses are obtained, by varying the synthesis conditions. PP were stored at room temperature. In absence of stabilizer, effects of light and/or air cause aging.
- Fresh virgin polypropylene (PP2), free of additives, have been synthesized in our laboratory using Ziegler-Natta catalysis. Different molar masses are obtained, by varying the synthesis conditions. PP have been stored in the fridge (+5°C) and away from light to avoid any potential thermal or photo degradation.
- A commercial PP (PP3), low in additives, has been purchased**.**

2.2. Chemicals

The used solvent was Spectropure dry 1,2,4 trichlorobenzene (TCB), purchased from BioSolve, and was used without further purification. Di-t-butylperoxide (DTBP) (as initiator)

and 2,6-Di-tert-butyl-4-methylphenol (BHT) (as antioxidant) were purchased from Sigma-Aldrich.

2.3. Dissolution and degradation vessel

Both dissolution and degradation were carried out in the same reactor. The equipment consists of a 500 mL glass jacketed vessel, heated by an oil bath. The vessel is equipped with a cooled condenser to condense any evaporated solvent. The medium was mixed by a 4-blades propeller. A 12 mm diameter Raman probe, a 6 mm NIR probe, and a temperature probe were inserted into the medium.

2.4. Experimental procedure of dissolution and degradation

For each experiment, the required amount of solvent was first introduced in the vessel. Then, the temperature was increased to the desired value using the heating bath. Once the temperature set point was reached, polypropylene was added (in pellet form or in powder form) at a known concentration. Polymer dissolution was carried out at a constant stirring rate (200 rpm). Argon or air was introduced in the sky of the vessel to avoid penetration of oxygen or to force oxidation of polypropylene, respectively. For some experiments, a peroxide (di-t-butylperoxide) was used to initiate/ enhance the degradation reaction. It was introduced to the reactor once complete polymer dissolution was reached, at a fraction of 0.4-1 wt% with respect to PP. The half-life of the peroxide ranges from 10 hours at 126°C to 1min at 193°C.

2.5. Sampling and reference method

Samples were collected at different intervals using a glass pipet previously heated with a heating band to avoid precipitation of polypropylene during the sampling. A uniform part of the sample was put in a vial. The vial was then immediately immersed in an ice bath to precipitate the polymer, and antioxidant (BHT) was added to stop further radical/oxidation reactions. Then, the polymer was completely precipitated and washed by methanol. The polymer powder was then recovered by filtration, and dried under vacuum at 110 °C and 104 Pa for 8 hours, followed by an additional drying at atmospheric pressure in an oven at 100 °C for 24 - 48 h. The polymer was then analyzed by high temperature size exclusion chromatography (HT-SEC).

2.6. Instruments

2.6.1. Raman spectroscopy

A Kaiser Optical Systems RXN2 Raman spectrometer, equipped with a 785 nm laser of 400 mW power, was used with an immersion probe of 12 mm in diameter. The acquisition conditions were as follow: 5 seconds of integration time, and 10 scans are averaged to give 1 spectrum each minute. The wavelength region ranges from 100 cm^{-1} to 3 425 cm^{-1}.

2.6.2. NIR spectroscopy

In-situ NIR analysis was performed using a Hellma-Falcata NEW XP6 immersion reflectance probe (Hellma GmbH & Co) of 6 mm diameter with an optical path fixed at 5 mm. The spectrometer NIRS MATRIX F-II (Bruker) recorded the spectra, at wavelengths within the 870 – 2 500 nm spectral range, with a resolution of 0.5 nm. Each final spectrum obtained was the average of 20 scans, leading to 1 spectrum each minute. The spectrometer was operated using the software OPUS (Bruker).

2.6.3. Size exclusion chromatography

Two high temperature size exclusion chromatography (HT-SEC) instruments were used due to availability reasons.

The first instrument was an HLC-8321 GPC/HT (Tosoh), with a differential refractive index (RI) detection. The stationary phase was a set of two Tosoh TSKgel GMHhr-H HT columns of 7.8 mm internal diameter x 300 mm length, containing 13 µm polymer beads. The injection volume was 300 µL and the flow rate 1 mL min^{-1}. Narrow dispersity polystyrene standards were used for calibration. The measurement was carried out at 150°C, with a sample concentration of 5 mg mL^{-1} of PP in the solvent TCB. Antioxidant BHT was added to the solvent reservoir in advance at a concentration of 0.4 g. L^{-1}. The used Mark-Houwink coefficients of polypropylene, K and $[\alpha]$, were 1.7×10^{-4} $dL.g^{-1}$ and 0.725, respectively.

The second instrument is a Polymer-Char GPC-IR (PolymerChar, Valencia, Spain). Detection was performed with a filter-based multiple band IR detector (model IR5-MTC, PolymerChar, Valencia,Spain). As stationary phase, three PLgel Olexis analytical columns, 7.5 × 300 mm (PolymerChar, Valencia, Spain) were used. The MMD was evaluated using polystyrene calibration (EasiCal PS-1, Agilent, Waldbronn, Germany). The used software was WinGPC version 8 (PolymerChar, Valencia, Spain). The instrument was equipped with a 200 µL sample loop, which corresponds to the injection volume. The mobile phase was 1,2,4 TCB, containing 0.4 g L^{-1} of BHT, and its flow rate was set at 1 mL min^{-1}. For each measurement, about 6 mg polymer was automatically dissolved in 8 mL of mobile phase. Simultaneously, the vials were flushed with nitrogen. Each sample was dissolved under shaking in the autosampler for 1 h at 150°C before injection. The molar masses of PS standards were transferred to polyethylene equivalents using the following Mark-Houwink coefficients: K_{PP}: 1.7×10^{-4} dL g–1, $[\alpha]_{PP}$: 0.725 and K_{PS}: 1.6×10^{-4} dL g^{-1}, $[\alpha]_{PS}$: 0.702.

Samples of batches 1 to 7 were analyzed with the Tosoh instrument, whereas samples of batches 8 to 17 were analyzed with the PolymerChar instrument.

2.6.4. *Polymer degradation experiments: operating conditions*

Different degradation batches were performed. The operating conditions were changed in order to build robust predictive models. Table 1 recapitulates the different operating conditions.

The table is organized by type of PP used: PP1 is the aged pure PP, PP2 is the fresh pure PP and PP3 is the commercial PP. The primary focus was on changing the temperature and the polymer concentration. Then, in some experiments, additional peroxide was added to force chain-scission, or additional antioxidant was added to avoid any chain-scission. The atmosphere was also changed by either working under air (so, in presence of oxygen to enhance oxidation) or working under argon to avoid any oxidation, thus limiting the chain-scission kinetics.

Finally, in order for the developed models covering a wide range of molar masses, the starting M_w has been changed.

- In the case of PP1, the starting molar mass depends on the synthesis conditions besides the aging conditions.
- In the case of PP2, the starting molar mass depends on the synthesis conditions, and care was made to avoid any change in M_w before the degradation study.
- In the case of PP3, the starting molar mass depends on the purchased polymer, which was found to remain unchanged until use.

At different time intervals during the degradation study, samples were taken to be analyzed by HT-SEC to measure the evolution of the molar mass. Also, Raman and NIR spectra were recorded in situ, to be related to the corresponding M_w reference measurement.

Table 1 Operating conditions of the polypropylene depolymerization experiment

Batch	Temp.	Conc.	Additional Peroxide	BHT	Atmosphere	PP type(a)	1st molar mass (M_w)(b)	2nd molar mass (M_w)(c)
	[°C]	[wt%]					[kg mol^{-1}]	[kg mol^{-1}]
1	130	10	No	No	Air	PP1	217.3	38.9
2	130	10	No	Yes	Ar	PP1	115.4	74.2
3	130	10	Yes	No	Air	PP1	173.4	143
4	150	5	No	No	Air	PP1	176.1	171.4
5	150	10	Yes	No	Ar	PP1	173.4	143
6	150	10	Yes	No	Air	PP1	240.5	172.2
7	150	15	No	No	Air	PP1	165.5	102
8	170	10	No	No	Air	PP1	191.2	96.3
9	170	10	Yes	No	Ar	PP1	187.9	139.9
10	150	10	Yes	No	Air	PP2	236.3	236.3
11	150	10	Yes	No	Air	PP2	177.3	177.3
12	150	10	Yes	No	Ar	PP2	232.1	232.1
13	170	10	Yes	No	Ar	PP2	232.1	232.1
14	170	10	No	No	Ar	PP2	102.8	102.8
15	130	10	No	Yes	Ar	PP3	249.4	249.4
16	150	10	Yes	No	Air	PP3	249.4	249.4
17	170	10	Yes	No	Air	PP3	249.4	249.4

(a) PP1 correspond to aged pure PP; PP2 to freshly synthesized pure PP; PP3 to commercial PP.

(b) 1st molar mass corresponds to the theoretical mass average molar mass (measured after synthesis or indicated by the supplier of the commercial PP).

(c) 2nd molar mass corresponds to the mass average molar mass measured just before degradation.

3. Results and discussion

3.1. Coloration during the degradation

Polypropylene degradation may involve chain scission and oxidation, leading to the formation of unsaturated double bonds and carbonyl groups respectively. Table 1 provides a detailed summary of the various operating conditions (batch 1 to batch 17) used in these degradation batches, including the type of PP (PP1, PP2, or PP3), temperature, atmosphere, and the presence of additives such as peroxide or antioxidants. These unsaturations can serve as precursors to chromophoric groups, contributing to a yellowing effect. Figure 1 shows the collected polymer at different sampling times for batch 1 (130°C, air) and batch 2 (130°C, argon, antioxidant). The change in color has only been observed during the degradation batches, specifically when chain-scission and oxidation occur, with the coloration becoming more intense when oxidation is present. This shift in color is likely related to the formation of degradation products, which could lead to an increase in fluorescence, that can be observed as a baseline drift in the *in-situ* Raman spectra.

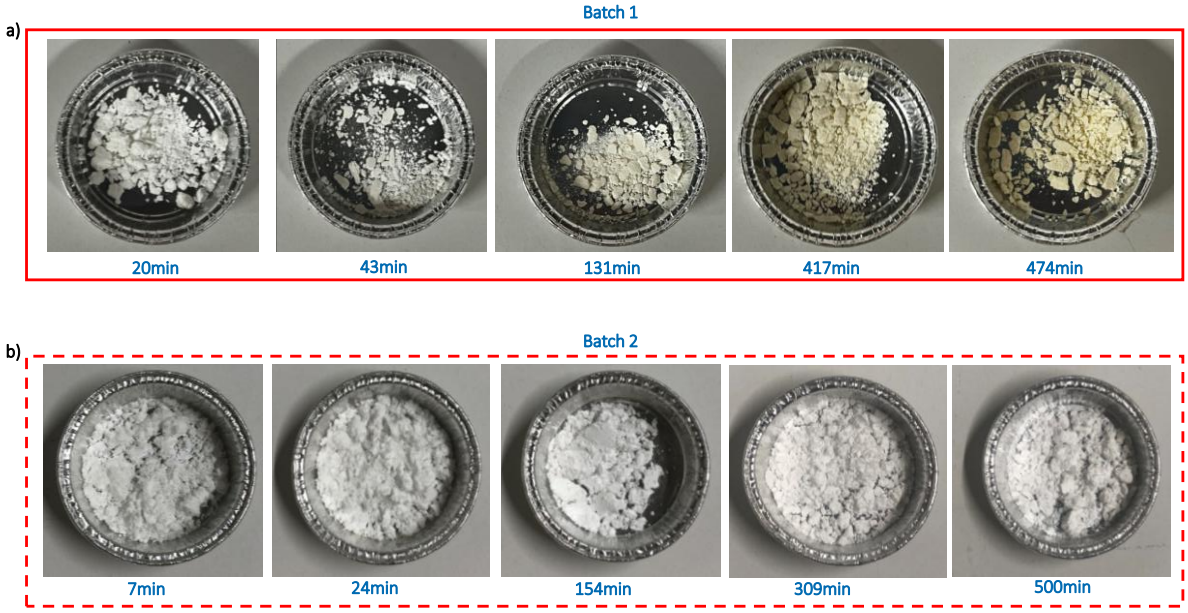

Figure 1 Yellowing effect (a) observed during batch 1 and (b) not observed during batch 2

3.2. Reference analysis: HT-SEC

Figure 2 shows the evolution of the molar mass distribution and the associated value of the mass average molar mass of the collected polymer from different samples of batches 1 and 2. A large decrease in the molar mass can be observed for batch 1, due to the chain scission phenomenon, while a negligible change is observed in batch 2.

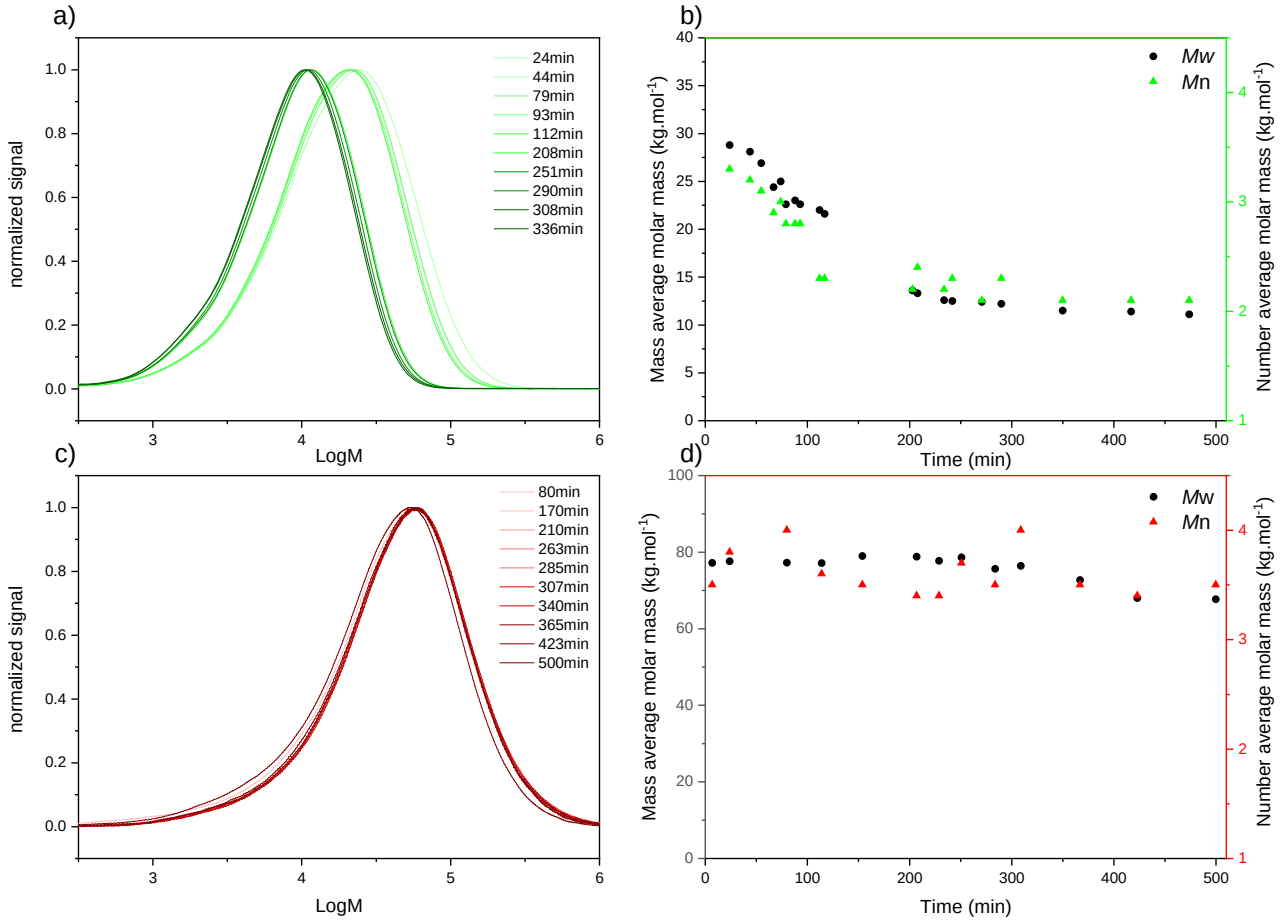

Figure 2 Molar mass distribution and associated mass average and number average molar mass during the degradation study of batch 1 ((a) and (b)), and batch 2 ((c) and (d)).

To be able to compare the molar mass evolution between the different batches (starting from different initial conditions), the chain-scission rate is calculated using Equation 1:

$$\text{chain scission rate}\ (\%) = 1 - \frac{Mw_{ti}}{Mw_{t0}} \times 100 \qquad (1)$$

Figure 3 shows the PP chain-scission rate, calculated from SEC experiments, for different degradation conditions (see Table 1). We can detect the non-degradation conditions corresponding to batches 2 and 15, where the molar mass remains relatively constant, because argon was used as well as the stabilizer BHT, and no peroxide was added. Batches 1, 5, and 9 to 11 show a slow degradation, due to the relatively mild degradation conditions (no stabilizer, but either air or a peroxide were added). The remaining batches 3, 4, 6 to 8, 12, 13, 16 and 17, show a fast degradation (observed without a stabilizer, with either air or a peroxide, or both). All these various degradation conditions provide a robust calibration set. The HT-SEC measurements for the different batches (M_n, M_w, $Đ$) are given in Tables S1 to S17.

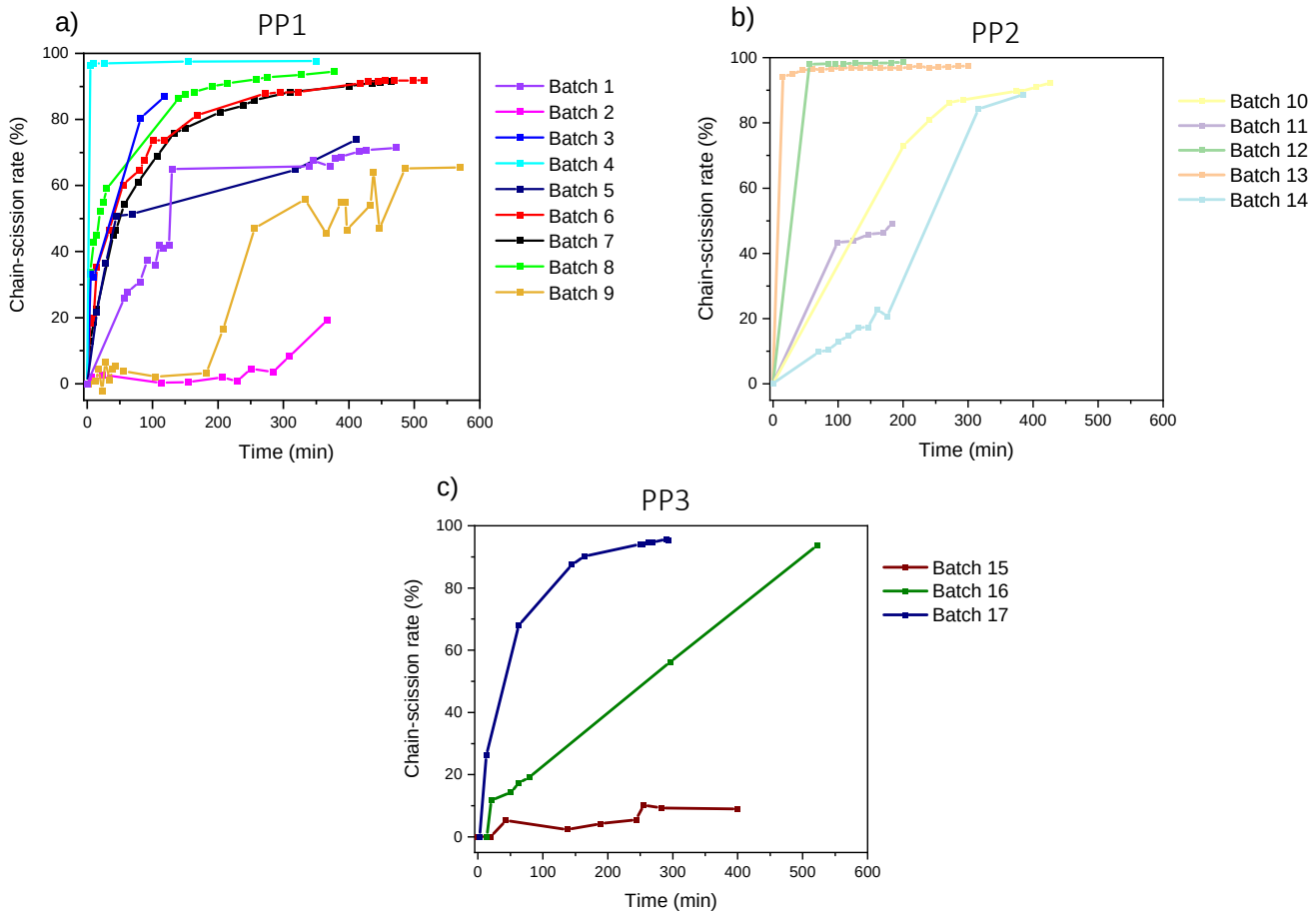

Figure 3 PP chain-scission rate under different chain-scission conditions for a) PP1: aged PP, b) PP2: fresh PP and c) PP3: commercial PP

3.3. In-situ spectroscopy analysis

3.3.1. Monitoring by Raman spectroscopy

For the Raman spectra, no specific algorithm was used for wavelength selection, but some regions were removed manually because they were noisy and lowering the model performances: 100 - 300 cm^{-1}, 1600 - 2700 cm^{-1} and 3200- 3425 cm^{-1}. The best performances (prediction error) was then obtained when preprocessing data with Standard Normal Variate and first derivative Savitzky-Golay, with a second polynomial order smoothing (SavGol[15,2,1]).

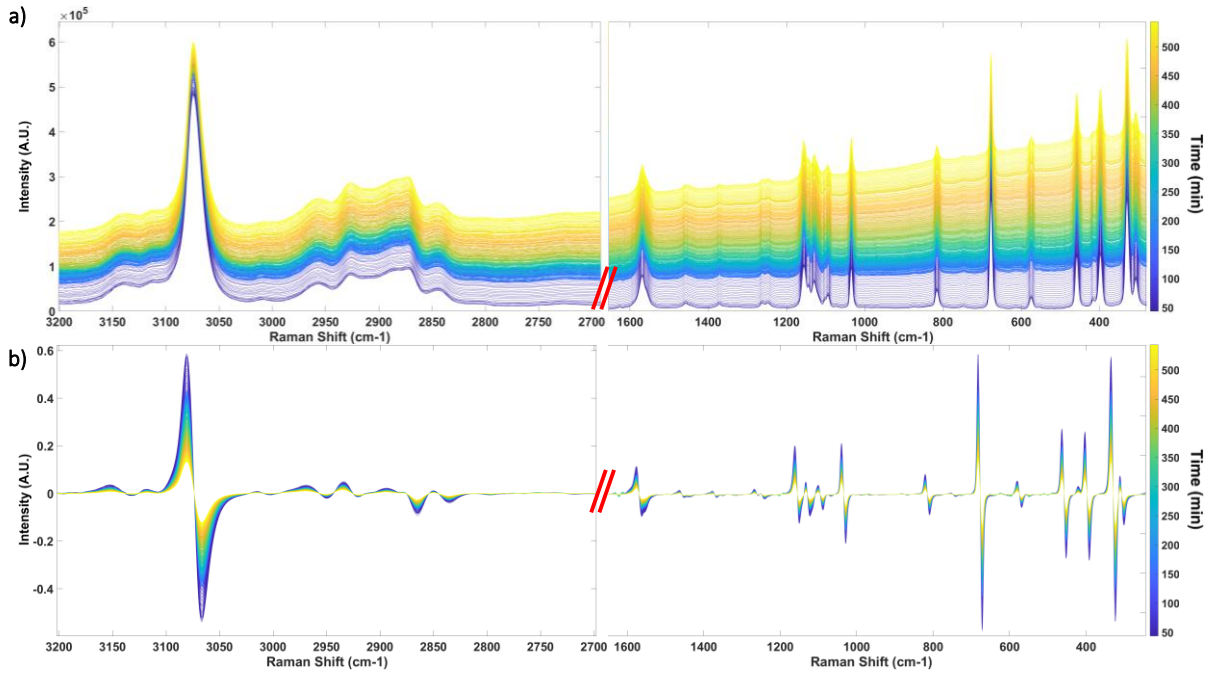

Figure 4 a) Raw Raman spectra and b) preprocessed Raman spectra during PP degradation in TCB at 150°C in batch 6 (which undergoes important degradation in M_w, from 172 to 6 kg.mol^{-1}).

The raw and preprocessed Raman spectra during the degradation of batch 3 are showed in Figure 4. The used preprocessing converted the baseline drift, to focus on the evolution of the band intensity (from Figure 4(a) to Figure 4(b)). Additionally, an orthogonalization preprocessing is used to remove other operating conditions that could affect the baseline. The band intensities are decreasing when the baseline drift is increasing, from blue to yellow, with time. This decrease is related to the baseline drift in the Raman spectra, which is primarily caused by fluorescence generation within the sample. This phenomenon is typically observed in the presence of conjugated double bonds or simple unsaturations, which is directly related to the chain-scission rate according to Figure 1. Indeed, the yellowing effect, generating fluorescence and creating the baseline drift, is possibly due to the presence of terminal vinylidene (from (A) to (G) in Figure S1) and carbonyl groups (from (A) to (D) in Figure S1), and is a good indicator of the chain-scission rate. The more the baseline drifts, the more the overall band intensities decrease, indicating a higher intensity of the chain-scission phenomenon. The change in the spectra is not a direct measurement of the polymer's molar mass but can indicate a variation in it. Indeed, Raman spectroscopy cannot reliably predict the molar mass of polymers in solution, as it primarily detects vibrational modes associated with the chemical structure, rather than the polymer chain length. Furthermore, the initial Raman spectra of the different batches are identical (exhibiting different molar masses), indicating that the Raman spectra are not directly related to the molar mass. As a result, it would be

more suitable to correlate it to the chain-scission rate calculated using Equation 1. Finally, no further wavelength selection was applied in Raman spectroscopy as the baseline drift is observed across all the spectrum, making it necessary to use the entire spectral range to capture the maximum amount of information. This approach helps mitigating the impact of the baseline drift by leveraging variations across all wavelengths, leading to more accurate predictions.

To develop a unique PLS model for the different operating conditions, orthogonal signal correction (OSC) preprocessing was applied to eliminate the effects of the different parameters (temperature, concentration, etc.). A PLS model was then built based on the selected regions after the indicated pre-processing method, using the PLS Toolbox v9.1 and MATLAB.

3.3.2. Monitoring by NIR spectroscopy

3.3.2.1. Sensitivity of NIR spectra to the polymer molar mass

NIR spectroscopy has greater potential for predicting the mass average molar mass. Indeed, NIR spectra capture overtones and combination bands that are sensitive to changes in polymer chain length and branching. This has already been investigated for instance during solution polymerization of methyl methacrylate [23, 24] or in a reactive extrusion process [25]. However, it should be noted that this phenomenon has often been predicted simultaneously with variations in other parameters, such as polymer conversion or particle size, so the variation on the NIR spectra might have been influenced by multiple factors, that can be correlated with the polymer molar mass. Therefore, these works do not demonstrate the effectiveness of molar mass measurement by the NIR.

In this study, straightforward prediction of the molar mass by NIR spectroscopy has been investigated. In our case, when degradation occurs, the change in the NIR spectra is primarily governed by the chain scission phenomenon, as the presence of carbonyl groups are not supposed not to significantly influence the NIR spectra. The impact of carbonyl groups on the NIR signal is minimal due to their low concentration in the polymer matrix. Additionally, the sensitivity of NIR to functional groups like carbonyls is relatively low compared to other spectroscopic techniques, which reduces the likelihood of any significant interference. So, we expect a bigger impact of chain scission on the spectral response. Furthermore, in batches 5, 9, 10, 11, 14 and 15 only chain scission occurs, so no oxidation is expected, thus helping the model to focus only on the molar mass changes. The pre-processed NIR spectra during batch 9 are shown in Figure 5. We can see those main variations on the spectra are related to a baseline change. Actually, NIR spectra obtained using diffuse reflectance or transmittance

frequently show different spectral responses when varying in the physical properties such as the particle size or the morphology such as surface roughness or shape. [26, 27] The most known wavelength-dependence effect is a baseline shift due to light scattering. It can thus be assumed, that for a specific molar mass distribution, light diffusion would be different for long chains and for short chains, especially when important changes occur. So, the calibration set was made on purpose to cover a large range of molar mass ranging from 250 kg.mol^{-1} (Table S15, batch 15 at t = 0 min, before degradation) to 4 kg.mol^{-1} (Table S10, batch 10 at t = 200 min, after degradation), to ensure a significative effect on the spectra, that can be correlated to the molar mass.

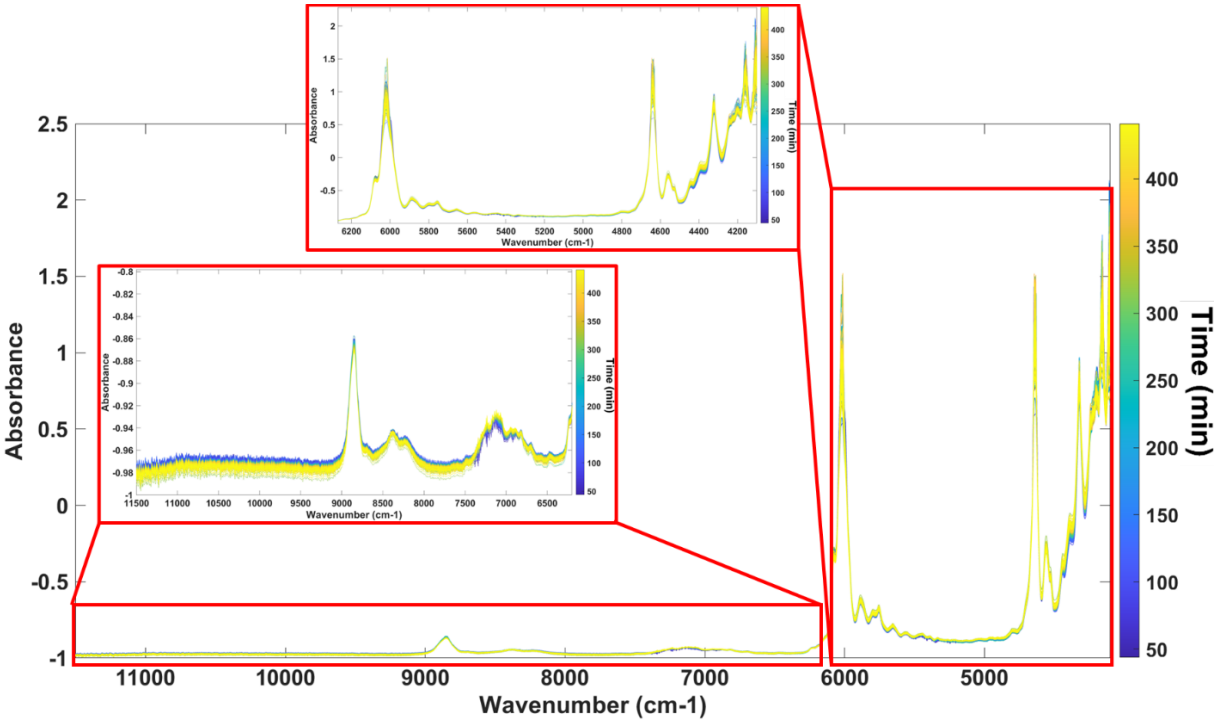

Figure 5 Preprocessed NIR spectra of PP degradation in TCB at 150°C in batch 9.

3.3.2.2. GA wavelength selection of NIR spectra

In NIR spectroscopy, careful wavelength selection enhances model accuracy by focusing on informative regions, minimizing noise and irrelevant spectral data, and improving robustness despite baseline variations.

Wavelength selection of NIR spectra has been performed by genetic algorithms (GAs). Genetic algorithms are well-known for their effective application on NIR spectra, particularly for automatic selection of relevant wavelengths. [28–30] The concept of genetic algorithms is based on a methodology inspired by natural selection, where a population of individuals (NIR spectra) undergoes reproduction, mutation, and selection operations to optimize a specific objective function (minimize the error during wavelength selection). [31] The parameters used

in the GA-PLS wavelength selection to get the minimum root mean square error of cross-validation (RMSECV) are presented in Table S18.

The retained wavelengths are shown in Figure S2 and include the following regions: 4 732-4 830 cm^{-1}, 5 132-5 230 cm^{-1}, 5 532-5 630 cm^{-1}, 5 732-5 830 cm^{-1}, 6 132-6 230 cm^{-1}, 6 832-7 130 cm^{-1}, 7 332-7 430 cm^{-1}, 7 932-8 030 cm^{-1}, 8 132-8 230 cm^{-1}, 8 432-8 530 cm^{-1}, 9 432-9 530 cm^{-1}, 11 232-11 330 cm^{-1}.

Then, a multiplicative signal correction (MSC (Mean)) was applied to the selected regions of the NIR spectra.

3.3.2.3. NIR molar mass model development

The number of latent variables (LVs) was determined based on the model quality indicators. Figure S3 shows the evolution of RMSEC and RMSECV as a function of the number of LVs for the NIR molar mass prediction model. The errors first decrease, then stabilize after 4 LVs. The use of GA wavelength selection improves the model quality which was detected from the reduction of the gap between the RMSEC and RMSEP.

The loadings of the PLS model were carefully examined to uncover the nature of the chemical or physical changes evidenced by the NIR data. Figure S4 shows the loadings of the first four latent variables. The second LV which represent 98 % of the variability corresponds to a baseline change. This is due to the MSC pretreatment, which normalizes scattering effects and shifts baseline-related variability to subsequent LVs. This suggests that light diffusion through the chains, of varying lengths during chain-scission experiments, is reflected on the baseline. Overall, no noisy LVs were retained (except the wavelength region around 5000 cm^{-1} and 7000 cm^{-1} on LV3 and LV4), indicating that the model is effectively capturing the relevant features of the data. A PLS model was then built to predict the polymer mass average molar mass with time.

3.3.2.4. Performances of Raman and NIR models

Figure 6 shows the parity plot for the molar mass prediction using NIR spectra and for the chain-scission rate prediction using Raman spectra. The total spectra set has been split into a calibration and a validation set, by removing all spectra of one batch for validation. The dashed lines represent the confidence interval compared to the reference measurement (i.e., HT-SEC), where a 10% error in the measured molar mass has been chosen. The associated model performances criteria are reported in **Table 2**. Both techniques show satisfying predictive performances with an error of 16 $kg.mol^{-1}$ for the NIR molar mass predicted and 19 % for the Raman chain-scission rate predicted

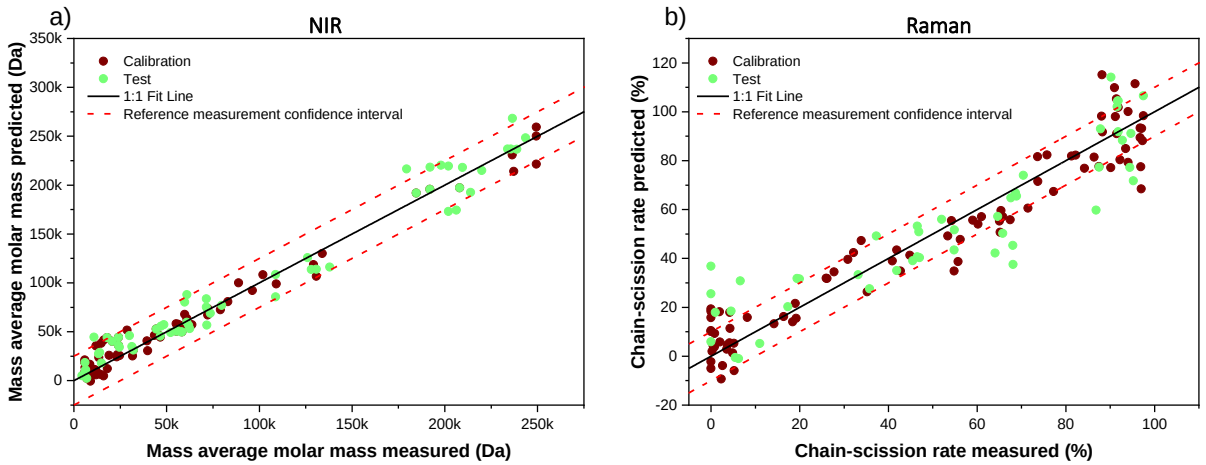

Figure 6: a) Parity plot of the HT-SEC measured molar mass vs. the NIR predicted molar mass and b), parity plot of the HT-SEC calculated chain-scission rate vs. the Raman predicted chain-scission rate.

Table 2 NIR and Raman model performances

	NIR	Raman
LVs	4	3
RMSEC	20000	12
RMSEP	22000	19
R^2C	0.984	0.900
R^2P	0.962	0.776

The low predictive squared correlation coefficient (R^2P) of the Raman model, can be explained by the irregular repartition of the values of the chain-scission rate. This is due to the definition of the chain-scission rate, causing a big number of extreme points (close to zero when degradation is negligible, and close to one hundred when degradation is completed what is never achieved). Also, remember that indirect effects on the baseline were corrected through orthogonalization preprocessing, to have identical initial Raman spectra of all batches (especially those of some polymers already partly degraded before the start of the experiment). These effects might not have been completely removed since some initial predictions have been out of the limits of the confidence interval. In the same way, predictions close to 100 % chain-scission rate are related to the final Raman spectra of the different batch, where the intensities of the bands become very low causing an error.

In the case of the molar mass NIR model, Figure 6(a) shows that out of 59 spectra predicted, 53 spectra were predicted within the confidence interval limits of the reference method, resulting in a prediction effectiveness of around 90 %. Also, the high value of the predictive squared correlation coefficient (R^2P) guarantees the reliability of the developed model for

making accurate predictions across the entire range of molar mass examined in this study. The entire range has been covered except between 150 kg.mol^{-1} and 200 kg.mol^{-1} due to an uncontrolled degradation and sampling could not be obtained in this range.

Regarding the effect of concentrations, the spectral observations suggest that these variations are not directly related to polymer content. We specifically chose polymer concentrations where we ensured that the polymer was fully dissolved. Therefore, the correlation in the model remains unaffected by polymer content.

The results indicate that the estimation of the molar mass and the chain-scission rate are possible, but a lower accuracy is expected in the case of the Raman chain scission rate model. This could be addressed by developing more robust predictive models that simultaneously use the information of the Raman spectra and the operating conditions in the framework of dynamic orthogonal projection (DOP) for instance. [32]

3.3.2.5. Predictive application of the developed model to monitor degradation

The developed models were then applied to monitor the solution degradation of polypropylene under different degradation (or non-degradation) conditions. Figure 7 shows the monitoring of batches 9, 15, 16 and 17 for which the temperature, the induced degradation and the addition of antioxidant have been changed, but all contain no stabiliser (Table 1).

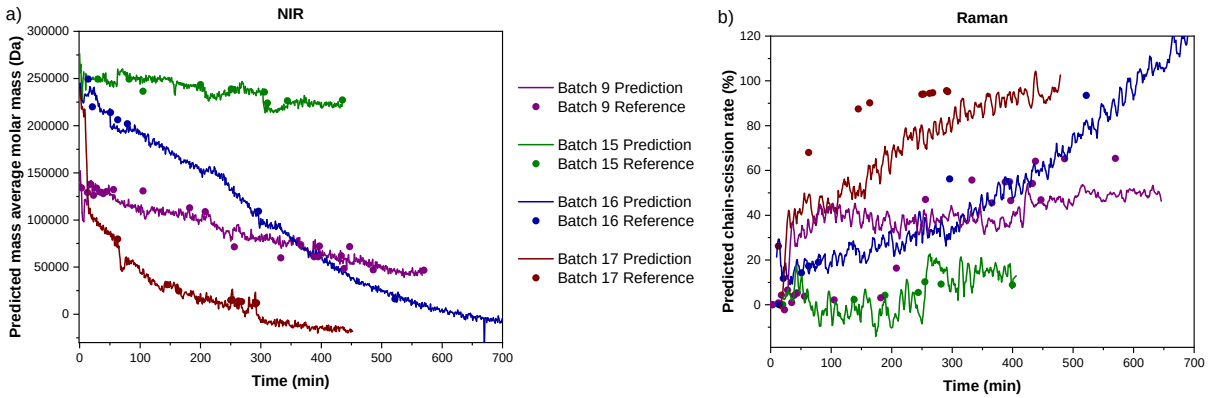

Figure 7: Prediction of the (a) mass average molar mass using NIR and (b) chain-scission rate using Raman during batch 9 (purple), batch 15 (green). batch 16 (blue) and batch 17 (red)

Overall, both spectroscopic techniques show that the real time monitoring of the chain-scission phenomenon is possible either by monitoring the mass average molar mass or the chain scission rate. More specifically for the NIR prediction (Figure 7(a)), a clear distinction between the different batches can be observed while for the Raman prediction (Figure 7(b)), the prediction is much noisier. As discussed above, this can be attributed first to the limited prediction range (from 0 to 100 %) and irregular repartition which force the model just to distinguish low (not degraded) from high values (severe degradation) of chain-scission. Secondly, the spectral signature of the Raman model is based on the baseline like in NIR, but

in Raman, the baseline drift (fluorescence) reaches a maximum (signal saturation) after which the spectra cannot not anymore be exploitable.

Nevertheless, in all batches, a global trend can be identified, and we can clearly differentiate batch 15 from the others which undergoes no degradation (PP3, low temperature, inert atmosphere). This is represented by a constant value of the molar mass over 8 hours and a chain-scission rate of less than 10 %.

Regarding the effect of oxygen, by comparing batch 17 (PP3, 170°C, peroxide, air) with batch 9 (PP1, 170°C, peroxide, argon), it can be observed that the degradation kinetics is logically higher in the presence of oxygen. Although the initial molar masses of the two batches were not identical, they can be compared in terms of their degradation kinetics. For batch 17, the molar mass decreases from 249.4 $kg.mol^{-1}$ to 11.9 $kg.mol^{-1}$ after 5 hours, while for batch 9 it decreases from 139 $kg.mol^{-1}$ to 60 $kg.mol^{-1}$. Oxygen accelerates indeed the degradation of polypropylene compared to argon by forming radicals in the air of the vessel, which induce chain scission and the formation of various degradation products. In contrast, argon slows down the degradation process by preventing the formation of oxidation products. Note that PP3 may contain some stabilizers (while PP1 is pure), but this did not protect it from degradation from degradation in the presence of air.

Regarding the effect of temperature, comparing batch 16 (PP3, 150°C, peroxide, air) and batch 17 (PP3, 170 °C, peroxide, air) demonstrate the impact of temperature on the chain-scission kinetics. By lowering the temperature from 170°C in batch 17 to 150°C in batch 16, we observed a slower change in the molar mass, and the chain-scission rate slowed down.

Both the Raman and NIR predictions are satisfactory: on one hand NIR can be used for the direct prediction of PP molar mass over a wide range; on the other hand, even with Raman spectroscopy, an analytical technique that is not sensitive to the molar mass in theory, it is possible to estimate a chain-scission rate indirectly through the fluorescence phenomenon.

3.3.2.6. Effect of initial aging on polypropylene depolymerization rate

The effect of initial aging on the depolymerization of polypropylene was investigated by comparing two degradation batches with relatively similar starting molar masses and the same operating conditions (150 °C, peroxide, air). **Figure 8** shows the monitoring of the molar mass by NIR spectroscopy during batch 6 (PP1, was synthesized at 240.5 $kg.mol^{-1}$, but after aging during storage a starting molar mass of 172.2 $kg.mol^{-1}$ was measured) and batch 11 (PP2, freshly synthesized with a starting molar mass of 177.3 $kg.mol^{-1}$). The results indicate a difference in the degradation rates between the two batches: the freshly synthesized PP degraded faster than the aged PP. This observation suggests that aging may influence the intrinsic stability of PP, possibly by altering its molecular structure or the distribution of chain

defects over time. The slower depolymerization rate in the aged PP could be attributed to a decrease in reactive sites for degradation and/or the formation of oxidation products over time, which may inhibit further degradation. In the same way, based on the chain-scission rates from Figure 3(a) of batch 4, where the polymer is aged but exhibits only a slight decrease in molar mass (PP1, was synthesized at 176.1 $kg.mol^{-1}$ and after aging during storage a starting molar mass of 171.4 $kg.mol^{-1}$ was measured), degrades the fastest. This suggests that even though the polymer is slightly aged, its reactivity remains high. This observation supports once that aged polymers tend to have slower degradation rates, likely due to fewer reactive sites available for chain scission. This highlights the importance of considering the aging history of PP when assessing its degradation behavior during dissolution-based recycling processes of PP wastes where polymer stability is critical.

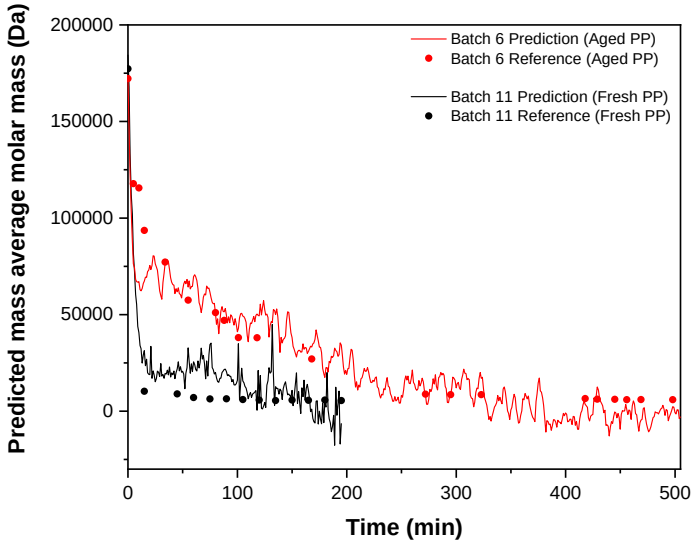

Figure 8: Prediction of the mass average molar mass during batch 6 and batch 11 using NIR spectroscopy.

3.3.2.7. About the possibility of using NIR spectroscopy for direct prediction of PP molar mass

To assess whether NIR spectroscopy could accurately determine the molar mass of various polymers based solely on their spectral data and determine the limiting ranges of operability, new polymers were prepared and evaluated by the model (not for the purpose of degradation). **Figure 8** shows the result of the prediction of the mass average molar mass of 6 external samples (with 3 replicates) not present in the calibration set. Theses samples correspond to PP2 (i.e., freshly synthesized PP where neither aging nor additives could impact the spectral response).

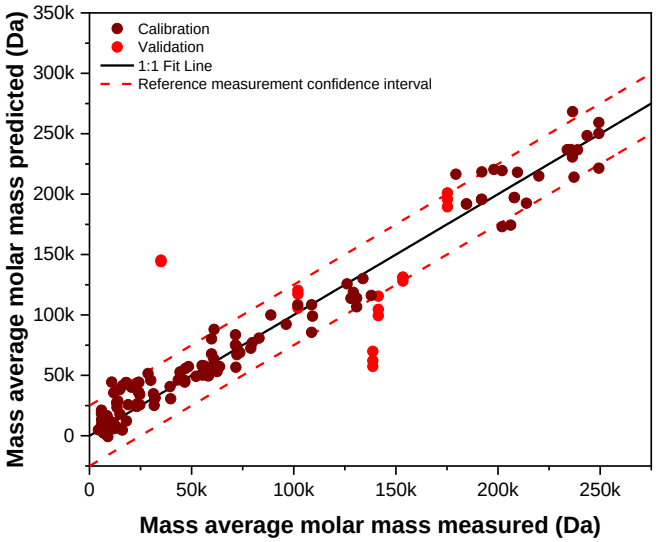

Figure 9: Prediction of the mass average molar mass of an external validation set using NIR spectroscopy.

Out of the 6 polymer samples tested, 3 samples (and their replicates) were predicted within the confidence interval of the reference measurement. For the remaining 3 samples, 1 was at the confidence limit, while the other 2 were predicted outside the confidence interval. While these results suggest that NIR spectroscopy has potential for predicting the mass average molar mass, the accuracy of the predictions remains questionable. This indicates that further refinement of the method is necessary to improve its precision, and limits may appear when little effect on the diffusion is obtained, or when other phenomena influence the diffusion. Future work could focus on optimizing the calibration models and exploring additional spectral preprocessing techniques to enhance the reliability and accuracy of NIR predictions for a broader range of polymer samples.

4. Conclusions

Mass average molar mass (M_w) values and chain-scission rates of polypropylene during dissolution in trichlorobenzene can be obtained directly from *in-situ* NIR and Raman spectra, respectively. The spectra are recorded under typical dissolution conditions of polymer dissolution-based recycling processes at elevated temperatures. Two chemometric models, based on partial least squares regression, were developed to predict these properties of the dissolution mixture. This has been enabled through a robust calibration set, considering variation in the polymer starting molar mass and employing various degradation rates at different temperatures, in the presence or not of peroxide or not oxygen. The spectral signature removal of the side effects in the initial composition by orthogonalization was important to focus only on the changes during the degradation experiments.

The model analysis revealed that the contribution to the NIR model was related to a baseline change that is correlated to light scattering, which varies differently depending on the length of the polymer chains. Moreover, the use of genetic algorithm (GA) has enabled the accurate wavelength regions selection of the NIR spectra, ensuring the best model predictions. In the case of the Raman model, the yellowing effect represented by a baseline drift due to fluorescence has been correlated to the chain-scission rate. Multivariate regression models were then developed for both spectroscopy methods.

The results suggest that while in-situ Raman and NIR spectroscopy PLS models provide quantitative data, their consistency and precision may vary compared to traditional ex-situ HT-SEC measurements, though they offer a faster and potentially automated alternative.

Some limitations in both techniques were however observed. The developed Raman/NIR-PLS model can be integrated into online process monitoring and control systems for dissolution step of PP recycling processes, enhance efficiency and accuracy in the recovery of high-quality polymers from waste materials.

Supporting Information

Supporting Information is available from the Wiley Online Library or from the author.

Author Contribution

S. Ferchichi: Conceptualization, Data acquisition, Model development, Writing – original draft. N. Sheibat-Othman: Conceptualization, Writing – reviewing, Supervision. O. Boyron: Polymer characterization. S. Norsic: Polymer synthesis. M. Rey-Bayle: Supervision. V. Monteil: Conceptualization, Writing – reviewing, Supervision. The manuscript was written through contributions of all authors. All authors have given approval to the final version of the manuscript.

Acknowledgements

The authors would like to thank IFP Energies Nouvelles for funding. The authors would like to thank Axel'One for providing the NIR spectrometer and the in-situ probe. The authors would like to thank Joao Pedro Florencio for the synthesis of pure polypropylene.

Graphical abstract

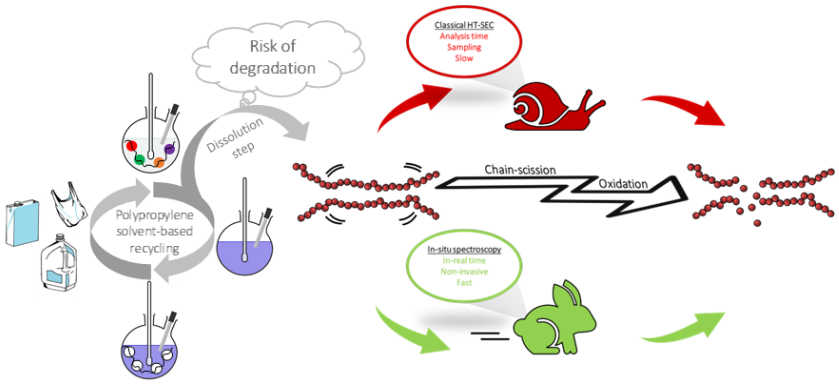

Highlights

Polypropylene degradation in solution

In-situ monitoring by Raman and NIR spectroscopy

Molar mass and chain-scission rate prediction

Monitoring during polypropylene dissolution-based recycling

References

[1] A. Chaudhary, M. Dave, D. S. Upadhyay, *Materials Today: Proceedings.* **2022**, *57*, 1730.
[2] G. Pappa, C. Boukouvalas, C. Giannaris, N. Ntaras, V. Zografos, K. Magoulas, A. Lygeros, D. Tassios, *Resources, Conservation and Recycling.* **2001**, *34*, 33.
[3] J. G. Poulakis, C. D. Papaspyrides, *Resources, Conservation and Recycling.* **1997**, *20*, 31.
[4] A. A. Shah, F. Hasan, A. Hameed, S. Ahmed, *Biotechnology Advances.* **2008**, *26*, 246.
[5] L. N. Shafigullin, N. V. Romanova, I. F. Gumerov, A. T. Gabrakhmanov, D. R. Sarimov, *IOP Conf. Ser.: Mater. Sci. Eng.* **2018**, *412*, 12070.
[6] G. Zhang, C. Nam, L. Petersson, J. Jämbeck, H. Hillborg, T. C. M. Chung, *Macromolecules.* **2018**, *51*, 1927.
[7] A. Hoff, S. Jacobsson, *J. Appl. Polym. Sci.* **1982**, *27*, 2539.
[8] C. Tzoganakis, Y. Tang, J. Vlachopoulos, A. E. Hamielec, *Polymer-Plastics Technology and Engineering.* **1989**, *28*, 319.
[9] A. Yoshiga, H. Otaguro, D. F. Parra, Lima, Luís Filipe C. P., A. B. Lugao, *Polym. Bull.* **2009**, *63*, 397.
[10] A. Chamas, H. Moon, J. Zheng, Y. Qiu, T. Tabassum, J. H. Jang, M. Abu-Omar, S. L. Scott, S. Suh, *ACS Sustainable Chem. Eng.* **2020**, *8*, 3494.
[11] N. S. Allen, M. Edge, *Fundamentals of polymer degradation and stabilisation*, London, New York, Elsevier Applied Science. **1992**.
[12] J. F. Rabek, *Polymer Photodegradation*, Dordrecht, Springer Netherlands. **1995**.
[13] S. H. Ryu, C. G. Gogos, M. Xanthos, *Advances in Polymer Technology.* **1991**, *11*, 121.
[14] H. Nakatani, Y. Ohshima, T. Uchiyama, S. Motokucho, *Sci Rep.* **2022**, *12*, 1.
[15] F. M. Coutinho, T. H. Costa, *Polymer Testing.* **1994**, *13*, 363.
[16] E. Niki, T. Shiono, T. Ido, Y. Kamiya, *J. Appl. Polym. Sci.* **1975**, *19*, 3341.
[17] M. Hoseini, J. Stead, T. Bond, *Environmental science. Processes & impacts.* **2023**, *25*, 2081.
[18] C. Rouillon, P.-O. Bussiere, E. Desnoux, S. Collin, C. Vial, S. Therias, J.-L. Gardette, *Polymer Degradation and Stability.* **2016**, *128*, 200.
[19] D. C. Mellor, A. B. Moir, G. Scott, *European Polymer Journal.* **1973**, *9*, 219.
[20] E. Syranidou, K. Karkanorachaki, D. Barouta, E. Papadaki, D. Moschovas, A. Avgeropoulos, N. Kalogerakis, *Environmental Science & Technology.* **2023**, *57*, 8130.
[21] X. Guo, Z. Lin, Y. Wang, Z. He, M. Wang, G. Jin, *Polymers.* **2019**, *11*.
[22] S. Ferchichi, N. Sheibat-Othman, O. Boyron, C. Bonnin, S. Norsic, M. Rey-Bayle, V. Monteil, *Anal. Methods.* **2024**, *16*, 3109.
[23] A. Cherfi, G. Févotte, *Macromolecular Chemistry and Physics.* **2002**, *203*, 1188.
[24] N. S. Othman, G. Févotte, D. Peycelon, J.-B. Egraz, J.-M. Suau, *AIChE J.* **2004**, *50*, 654.
[25] B. Bergmann, W. Becker, J. Diemert, P. Elsner, *Macromol. Symp.* **2013**, *333*, 138.
[26] M. Otsuka, A. Koyama, Y. Hattori, *RSC Adv.* **2014**, *4*, 17461.
[27] A. Kuriyama, J. Osuga, Y. Hattori, M. Otsuka, *AAPS PharmSciTech.* **2018**, *19*, 710.
[28] J. Tan, Y. Sun, L. Ma, H. Feng, Y. Guo, W. Cai, X. Shao, *Chemometrics and Intelligent Laboratory Systems.* **2020**, *206*, 104150.
[29] D. D. Silalahi, C. E. Reaño, F. P. Lansigan, R. G. Panopio, N. C. Bantayan, *Information Processing in Agriculture.* **2016**, *3*, 252.
[30] Q. Ding, G. W. Small, M. A. Arnold, *Anal. Chem.* **1998**, *70*, 4472.
[31] A. S. Bangalore, R. E. Shaffer, G. W. Small, M. A. Arnold, *Anal. Chem.* **1996**, *68*, 4200.
[32] M. Zeaiter, J. M. Roger, V. Bellon-Maurel, *Chemometrics and Intelligent Laboratory Systems.* **2006**, *80*, 227.

Supporting Information

Polypropylene chain-scission in solution monitored by near infrared and Raman spectroscopy.

Sofiane Ferchichi[a,b,c], *Nida Sheibat-Othman*[b*], *Olivier Boyron*[c], *Sébastien Norsic*[c], *Maud Rey-Bayle*[a], *Vincent Monteil*[c*]

[a]IFP Energies Nouvelles, Rond-Point de l'échangeur de Solaize, 69360 Solaize, France

[b]Universite Claude Bernard Lyon 1, LAGEPP, UMR 5007, CNRS, 69622 Villeurbanne, France

[c]Universite Claude Bernard Lyon 1, CP2M, UMR 5128, CNRS, 69616 Villeurbanne, France

E-mail: Vincent.MONTEIL@univ-lyon1.fr, nida.othman@univ-lyon1.fr

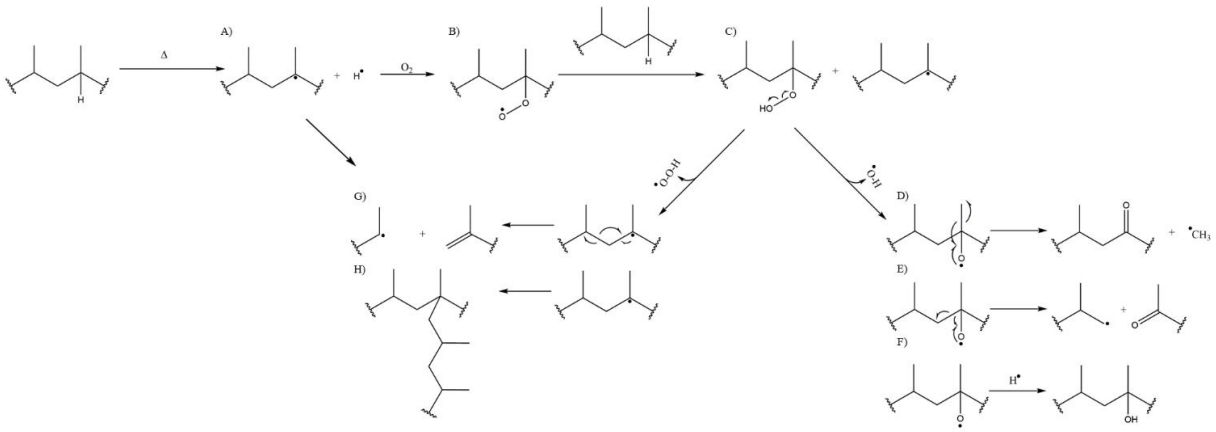

Figure. S1Thermal and oxidative degradation of polypropylene, adapted from [6]

Table. S1 Number-average molar mass (M_n), mass-average molar mass (M_w), and dispersity ($Đ$) of the samples during Batch 1

Time	M_n	M_w	$Đ$
[min]	[kg.mol^{-1}]	[kg.mol^{-1}]	
0	9.7	38.8	3.9
57	8.6	28.8	3.3
62	8.6	28.1	3.2
81	8.6	26.9	3.1
92	8.3	24.4	2.9
104	8.3	25.0	3.0
111	8.0	22.6	2.8
116	8.1	23.0	2.8
125	8.1	22.6	2.8
130	5.7	13.6	2.3
340	5.7	13.3	2.3
345	5.6	12.6	2.2
371	5.5	13.3	2.4
379	5.5	12.4	2.2
388	5.3	12.2	2.3
416	5.3	11.5	2.1
427	5.0	11.4	2.3
473	5.0	11.1	2.1

Table. S2 Number-average molar mass (M_n), mass-average molar mass (M_w), and dispersity ($Đ$) of the samples during Batch 2

Time	*M*n	*M*w	*Đ*
[min]	[kg.mol^{-1}]	[kg.mol^{-1}]	
0	15.3	74.2	4.8
7	22.0	77.6	3.5
24	20.0	77.2	3.8
114	19.6	79.0	4.0
154	21.3	78.8	3.6
207	21.5	77.7	3.5
229	22.5	78.6	3.4
251	21.9	75.6	3.4
284	20.2	76.4	3.7
309	20.4	72.7	3.5
367	16.0	64.0	4.0

Table. S3 Number-average molar mass (M_n), mass-average molar mass (M_w), and dispersity ($Đ$) of the samples during Batch 3

Time	*M*n	*M*w	*Đ*
[min]	[kg.mol^{-1}]	[kg.mol^{-1}]	
0	37.6	143.3	3.8
6	19.7	95.7	4.8
10	23.9	97.2	4.1
82	9.4	28.0	2.9
118	5.4	18.8	3.4

Table. S4 Number-average molar mass (M_n), mass-average molar mass (M_w), and dispersity ($Đ$) of the samples during Batch 4

Time	M_n	M_w	$Đ$
[min]	[kg.mol^{-1}]	[kg.mol^{-1}]	
0	32.4	171.4	5.3
5	2.2	6.0	2.7
10	2.0	5.2	2.5
26	2.0	5.2	2.5
154	1.6	4.3	2.6
350	1.5	4.0	2.6

Table. S5 Number-average molar mass (M_n), mass-average molar mass (M_w), and dispersity ($Đ$) of the samples during Batch 5

Time	M_n	M_w	$Đ$
[min]	[kg.mol^{-1}]	[kg.mol^{-1}]	
0	37.6	143.3	3.8
15	31.0	112.3	3.6
29	16.9	91.0	5.3
45	21.7	70.6	3.2
69	13.2	69.7	5.2
318	14.4	50.5	3.5
411	9.2	37.3	4.1

Table. S6 Number-average molar mass (M_n), mass-average molar mass (M_w), and dispersity ($Đ$) of the samples during Batch 6

Time	M_n	M_w	$Đ$
[min]	[kg.mol^{-1}]	[kg.mol^{-1}]	
0	15.2	172.2	4.7
5	15.3	58.9	3.8
10	16.8	57.8	3.4
15	14.7	46.8	3.1
34	13.8	38.6	2.8
55	10.1	28.7	2.8
80	9.5	25.5	2.6
88	9.3	23.5	2.5
101	7.5	19.0	2.5
118	8.0	19.0	2.3
168	13.5	13.5	2.5
272	3.7	8.8	2.3
295	3.6	8.5	2.3
323	3.8	8.5	2.2
418	2.9	6.5	2.2
429	2.6	6.2	2.3
445	2.7	6.1	2.2
456	3.3	5.9	2.0
469	2.9	6.0	2.1
498	2.8	5.9	2.1
516	2.8	5.9	2.0

Table. S7 Number-average molar mass (M_n), mass-average molar mass (M_w), and dispersity ($Đ$) of the samples during Batch 7

Time	M_n	M_w	$Đ$
[min]	[kg.mol^{-1}]	[kg.mol^{-1}]	
0	26.3	102.0	3.8
5	26	88.8	3.4
10	23.7	83.0	3.5
15	25.1	79.0	3.1
40	18.5	56.2	3.0
44	19.6	54.6	2.7
57	18.4	46.7	2.5
78	17.0	39.8	2.3
107	14.0	31.7	2.2
133	10.8	24.7	2.2
150	10.2	23.2	2.3
203	8.4	18.1	2.1
239	7.4	16.1	2.1
256	6.7	14.4	2.1
310	5.5	12.0	2.1
400	4.7	10.0	2.2
435	4.4	9.2	2.0
448	4.4	9.0	2.0
465	4.3	8.7	1.9

Table. S8 Number-average molar mass (M_n), mass-average molar mass (M_w), and dispersity ($Đ$) of the samples during Batch 8

Time	M_n	M_w	$Đ$
[min]	[kg.mol^{-1}]	[kg.mol^{-1}]	
0	22.1	96.3	4.3
5	20.3	63.7	3.1
10	20.2	55.2	2.7
15	20.3	53.1	2.6
20	17.2	46.2	2.6
25	15.6	43.5	2.7
30	15.6	39.5	2.5
140	6.3	13.1	2.0
150	5.5	12.0	2.2
164	5.5	11.3	2.0
191	4.7	9.7	2.0
215	4.2	8.8	2.0
259	3.7	7.5	1.9
276	3.5	6.9	2.0
328	3.3	6.3	1.9
378	2.8	5.3	1.9

Table. S9 Number-average molar mass (M_n), mass-average molar mass (M_w), and dispersity ($Đ$) of the samples during Batch 9

Time	M_n	M_w	$Đ$
[min]	[kg.mol^{-1}]	[kg.mol^{-1}]	
0	22.5	139.9	6.2
3	20.3	133.9	6.5
13	19.2	129.2	6.7
18	22.4	138.0	6.1
23	20.9	126.1	6.0
28	21.6	133.7	6.2
35	21.4	129.3	6.0
39	21.2	128.0	6.0
44	21.4	129.9	6.0
56	21.3	132.1	6.2
105	19.8	130.8	6.5
182	20.4	112.9	5.5
208	20.2	108.8	5.3
256	15.5	71.5	4.6
333	14.1	59.8	4.2
366	16.7	73.6	4.4
388	14.1	61.0	4.3
395	14.3	60.9	4.2
397	16.9	72.2	4.2
433	16.2	62.9	3.8
438	12.8	48.5	3.7
447	17.4	71.7	4.1
486	12.4	47.0	3.7
570	12.9	46.7	3.6
609	14.1	48.0	3.4

Table. S10 Number-average molar mass (M_n), mass-average molar mass (M_w), and dispersity ($Đ$) of the samples during Batch 10

Time	M_n	M_w	$Đ$
[min]	[kg.mol^{-1}]	[kg.mol^{-1}]	
0	28.9	236.3	9.5
56	2.7	5.6	2.1
86	2.6	5.3	2.0
96	2.2	5.0	2.2
108	2.4	5.1	2.0
126	2.4	4.9	2.0
158	2.4	4.8	2.0
182	2.0	4.4	2.1
200	2.0	4.0	1.9

Table. S11 Number-average molar mass (M_n), mass-average molar mass (M_w), and dispersity ($Đ$) of the samples during Batch 11

Time	M_n	M_w	$Đ$
[min]	[kg.mol^{-1}]	[kg.mol^{-1}]	
0	20,.6	177,.3	8.6
15	4.3	10,.3	2.3
30	3.9	8.9	2.2
45	3.2	7.0	2.2
60	2.7	6.3	2.3
75	3.0	6.4	2.2
90	2.9	6.0	2.1
105	2.8	5.7	2.1
120	2.7	5.5	2.1
135	2.8	5.7	2.1
150	2.4	5.6	2.3
165	2.8	5.7	2.1
180	2.7	5.5	2.1
195	2.9	5.7	1.9
210	2.7	5.3	1.9
225	2.3	4.5	1.9
240	2.9	5.7	1.9
255	2.6	5.1	1.9
270	2.2	4.9	2.1
285	2.4	4.8	2.0
300	2.3	4.4	2.0

Table. S12 Number-average molar mass (M_n), mass-average molar mass (M_w), and dispersity ($Đ$) of the samples during Batch 12

Time	M_n	M_w	$Đ$
[min]	[kg.mol^{-1}]	[kg.mol^{-1}]	
0	26.6	232.1	8.7
70	34.2	209.5	6.1
86	31.4	208.0	6.6
101	33.1	202.0	6.1
116	34.1	198.0	5.8
131	36.5	192.1	5.2
146	39.1	192.0	4.9
161	32.6	179.4	5.5
176	33.6	184.0	5.5
316	14.5	36.7	2.5
385	10.0	26.2	2.6

Table. S13 Number-average molar mass (M_n), mass-average molar mass (M_w), and dispersity ($Đ$) of the samples during Batch 13

Time	M_n	M_w	$Đ$
[min]	[kg.mol^{-1}]	[kg.mol^{-1}]	
0	26.6	232.1	8.7
201	13.2	62.5	4.7
241	11.1	44.4	4.0
271	8.1	32.1	3.9
292	8.5	30.0	3.5
374	6.5	24.1	3.7
382	7.3	24.0	3.2
405	6.3	20.7	3.2
427	5.4	18.0	3.3

Table. S14 Number-average molar mass (M_n), mass-average molar mass (M_w), and dispersity ($Đ$) of the samples during Batch 14

Time	M_n	M_w	$Đ$
[min]	[kg.mol^{-1}]	[kg.mol^{-1}]	
0	13.1	102.8	7.8
99	14.2	58.3	4.1
123	12.8	57.8	4.5
147	13.6	55.7	4.1
170	13.4	55.2	4.1
183	11.2	52.2	4.6

Table. S15 Number-average molar mass (M_n), mass-average molar mass (M_w), and dispersity ($Đ$) of the samples during Batch 15

Time	M_n	M_w	$Đ$
[min]	[kg.mol^{-1}]	[kg.mol^{-1}]	
0	22.5	249.4	11.1
43	24.4	236.5	9.7
138	23.9	243.6	10.2
189	21.5	238.9	11.1
244	24.6	235.7	9.5
255	24.7	233.9	9.4
282	23.2	236.4	10.1
400	23.7	237.2	9.9

Table. S16 Number-average molar mass (M_n), mass-average molar mass (M_w), and dispersity ($Đ$) of the samples during Batch 16

Time	M_n	M_w	$Đ$
[min]	[kg.mol^{-1}]	[kg.mol^{-1}]	
0	22.5	249.4	11.1
14	24.0	222.0	9.2
21	25.6	213.9	8.3
51	22.8	206.2	9.0
63	24.4	202.0	8.2
296	8.4	109.2	13.6
522	3.6	16.2	4.7

Table. S17 Number-average molar mass (M_n), mass-average molar mass (M_w), and dispersity ($Đ$) of the samples during Batch 17

Time	M_n	M_w	$Đ$
[min]	[kg.mol^{-1}]	[kg.mol^{-1}]	
0	22.5	249.4	11.1
13	24.1	184.1	7.6
63	18.8	79.7	4.2
145	10.8	31.3	2.8
164	9.7	24.6	2.5
250	6.5	14.9	2.3
253	6.7	14.8	2.2
263	6.4	13.9	2.1
268	6.3	13.3	2.1
291	5.6	10.9	1.9
293	5.5	11.9	2.1

Table. S18 Optimal Genetic algorithm configuration

GA parameter	
Population size	256
Window width	50
Mutation rate	0.01
Crossover	Double
% at convergence	90
Regression	PLS with 4 max. Latent Variables

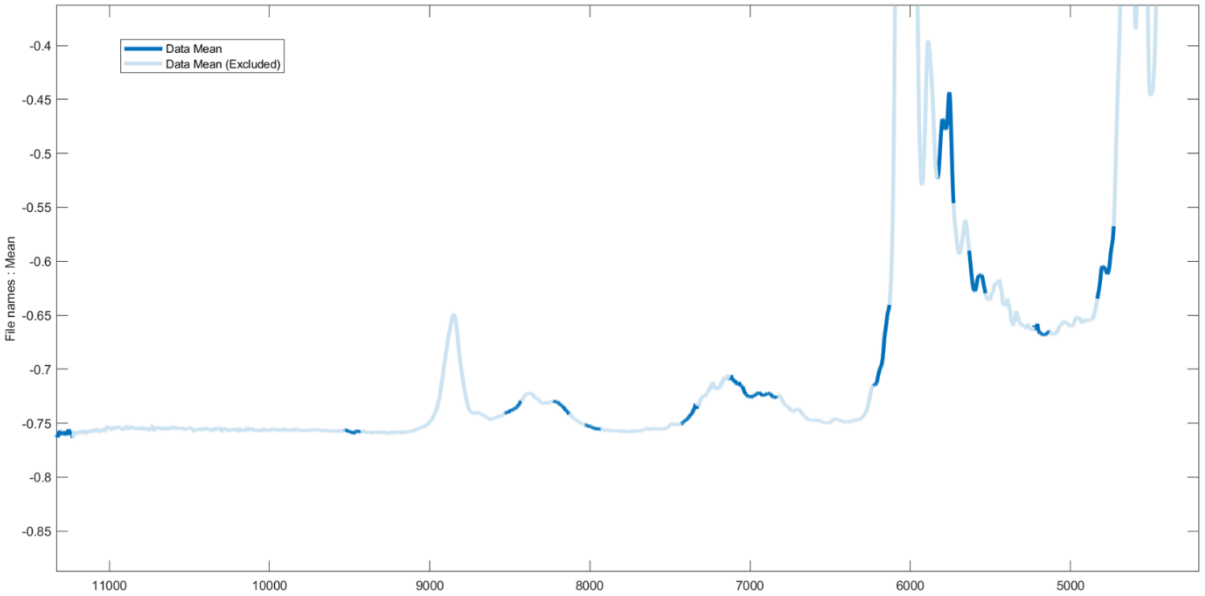

Figure. S2 Selections of wavelength regions using GA. The dark blue represents the selected regions while the light blue represents the excluded regions. The variable selection is applied to all the experiments

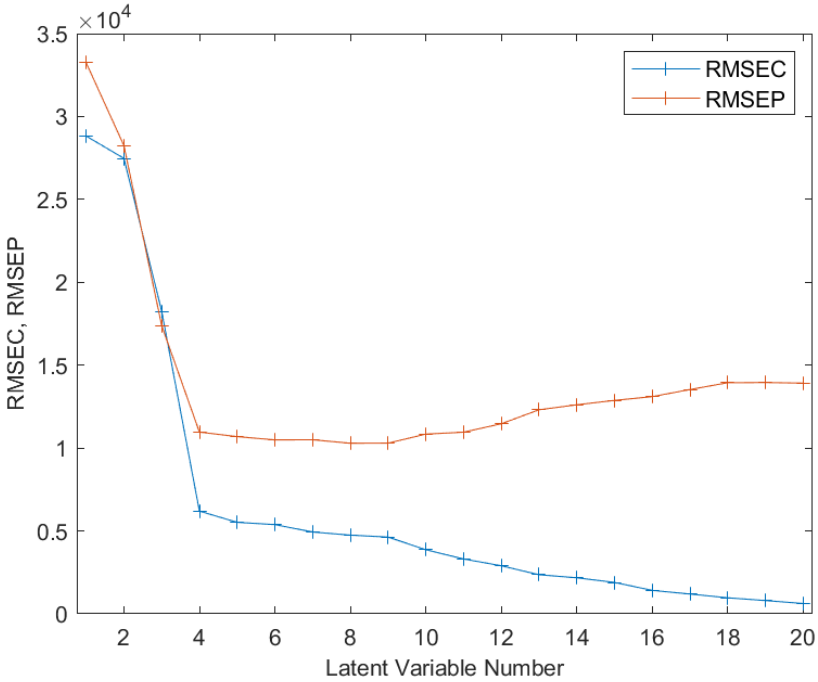

Figure. S3RMSEP vs RMSEC for the NIR model

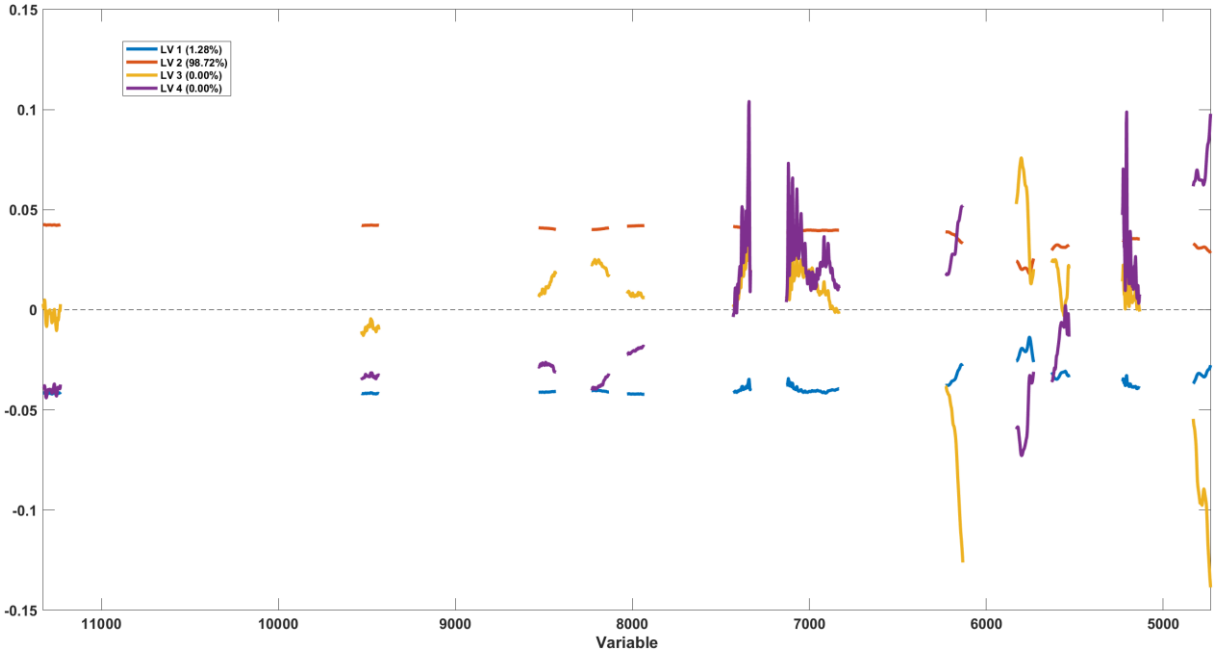

Figure. S4 Four first latent variables of the NIR model